

Coupled MHD Stellar and Disk Winds: Application to Planetary Nebulae

Eric G. Blackman^{1,2}, Adam Frank¹, and Carl Welch¹

1. Department of Physics & Astronomy, University of Rochester, Rochester, NY 14627
2. ITP, University of California, Santa Barbara, CA 93106

(submitted to ApJ)

Abstract

MHD winds can emanate from both stars and surrounding disks. When the two systems are coupled by accretion, it is of interest to know which (if either) of the two dominates the outflow power. Recent observations lead us to consider how such coupled MHD winds may be operating in planetary nebulae (PN). In this context, we calculate the MHD wind power from a coupled disk and star, where the former results from binary disruption. The resulting wind powers depend only on the accretion rate and stellar properties. We find that if the stellar envelope were initially slowly rotating, the disk wind would dominate throughout the evolution. If the envelope of the star were rapidly rotating, the stellar wind could initially be of comparable power to the disk wind until the stellar wind carries away the star's angular momentum. Since an initially rapidly rotating star can have its spin and magnetic axes misaligned to the disk, multipolar outflows can result from this disk wind system. For times greater than a spin-down time, the post-AGB stellar wind is slaved to the disk for both slow and rapid initial spin cases and the disk wind luminosity dominates. We find a reasonably large parameter space where a hybrid star+disk MHD driven wind is plausible and we discuss the morphologies which may emerge. The coupled winds might help explain the shapes of a number of remarkable multi-shell or multi-polar nebulae. Magnetic activity such as X-ray flares may be associated with the both central star and the disk and would be a valuable diagnostic for the dynamical role of MHD processes in PNe.

Subject headings: jets and outflows; accretion, accretion disks; planetary nebulae: general; ISM: magnetic fields: MHD; stars: AGB and post-AGB

1. Introduction

Planetary Nebulae (PNe) and proto-Planetary Nebulae (PPNe) are believed to be the penultimate evolutionary stage of low and intermediate mass stars ($M_* \leq 1 M_\odot \text{ yr}^{-1}$). PNe appear on the sky as expanding ionized plasma clouds surrounding a hot central star. As the resolution of ground based telescopes increased, the “typical” shape of a PN went from spherical (Osterbrock 1972) to ellipitcal and/or bipolar (Balick 1987). More recently, deeper and higher resolution studies (particularly those with the HST) have shown many PNe with narrow collimated features that are better described as *jets* than *bipolar lobes*. In some cases the jets appear as extremely well collimated bipolar outflows: M2-9 (Balick 2000): Hen-401 (Sahai 2000), AFGL 2688 (The Egg) (Sahai *et al.* 1998). In other cases they appear as FLIERS (Fast Low-Ionization Emission Regions), a single knot expanding away from a (usually) elliptical nebula. In addition to the presence of jets it also appears that many PNe show evidence for multi-shell structures or multi-polarity. In these objects two nested pairs of bipolar lobes appear. In multi-shell structures the lobes are aligned along the same axis of symmetry (Hb 12: Welch *et al.* 1999) while multi-polar cases show different orientations for the inner and outer lobes (M2-46: Manchado *et al.* 2000).

While considerable progress has been made in understanding the the hydrodynamics or magneto-hydrodynamics of shaping bipolar lobes (see Frank 1999 for a review), the origin of jets, point symmetry and multi-polar outflows in PNe poses fundamental challenges for theory.

The basic hydrodynamics of bipolar outflows can be decribed by the classic Generalized Interacting Stellar Winds (GISW) model (Kwok *et al.* 1978, Kahn & West 1986, Balick 1987, Icke 1988). In this scenario a slow (10 km s^{-1}), dense ($10^{-4} M_\odot \text{ yr}^{-1}$) toriodal wind expelled during the AGB is followed by a fast (1000 km s^{-1}), tenuous ($10^{-7} M_\odot \text{ yr}^{-1}$) wind driven off the contracting proto-white dwarf during the PNe phase. The GISW model can explain bipolar morphologies and even jets. Point-symmetry and multipolar bubbles however, do not fall easily into line with the concept of a large-scale collimating torus.

Models invoking a toroidal magnetic field embedded in a normal radiation driven stellar wind have recently shown some promise. This so-called *Magnetized Wind Bubble (MWB)* model was first proposed by (Chevalier & Luo 1994) and has been studied numerically by (Rozyczka & Franco 1996) and (Garcia-Segura *et al.* 1999). In these models the field at the star is dipolar but assumes a toroidal topology due to rapid stellar rotation. Collimation is not activated until the wind passes through the inner shock. Then hoop stresses associated with the toroidal field dominate over isotropic gas pressure forces and material is drawn towards the axis producing a collimated flow. This mechanism has been shown capable of producing a wide variety of outflow morphologies including well collimated jets. When

precession of the magnetic axis is included in fully 3-D simulations, the MWB model is capable of recovering point-symmetric morphologies as well (Garcia-Segura 1997). Potential difficulties with these models are the rather extreme single star input parameters (rotation rates and magnetic fields) required for the hoop stresses to become effective. It is noteworthy that the wind in these models differs substantially from standard MHD driven winds in disk and stellar wind contexts, and the fundamental issue of collimation before the wind-wind interaction remains to be addressed. In addition it is not clear that such models can be applied to multi-polar bubbles due to the difference in collimation orientations.

Finally neither the GISW or MWB models fully address the origin of the wind. This becomes a critical issue when one is dealing with Proto-PNe (PPNe). There is growing evidence suggesting that the PN shaping process begins in the PPN phase via well collimated jets (Sahai & Trauger 1998). The creation of fast ($V > 100$ km/s) high mass loss rate ($\dot{M} > 10^{-6} M_{\odot}$ yr $^{-1}$) winds during these early phases when the star is an F or G type is not easily explained via classic line driven wind theory. Thus for PPN, theorists face a dilemma similar to the problem of YSO outflows in that they must explain *both* wind acceleration and collimation (Pudritz 1991, Königl, A., & Ruden 1993, Shu *et al.* 1994)

The above considerations have motivated further study of magnetized wind models for the launching and collimation of outflows from PN. Magnetically driven outflows are a leading paradigm for a ubiquity of source classes in nature. This includes such contexts as protostellar jets (c.f. Smith 1998; Frank 1999 for reviews), the Solar wind (c.f. Parker 1979), jets of Galactic accretors (c.f. Mirabel and Rodriguez 1999), active galactic nuclei (c.f. Ferrari 1998; Blandford 2000 for reviews), and gamma-ray bursts (e.g. Usov 1992; Blackman *et al.* 1996; Meszaros & Rees 1997). While the parameter regimes are varied and the extent and nature of collimation, particle acceleration, and radiation process are different in the different settings, an underlying principle remains: magnetic fields can act as a drive belt between gravity and energy deposition at large radii, extracting the rotational energy of the rotator into an outflow. We note that the potential for accretion disks to exist in PPN systems has been raised by (Morris 1987) and (Soker & Livio 1994).

In the case of PN, as in other star-disk or compact object-disk systems, the magnetically driven outflows can in principle emanate from both the central object or the disk. It is important, therefore, to understand which object produces a wind and how the outflow system would manifest if both star and disk produced concurrent winds. Because the relative collimation and power evolution of the disk and stellar winds can be different, it may not be unreasonable to see outflows of different character coexisting in the same object. In order to investigate this properly however, it is necessary to allow that the disk and star are coupled and this requires a model for the disk evolution.

A careful investigation of one form of disk formation in pre-planetary nebula systems is presented in Reyes-Ruiz & Lopez (1999). The disks in their study form when a binary system undergoes common envelope evolution. The ejection of the envelope involves transfer of angular momentum from the secondary to the envelope after which the secondary loses enough mass to fall to a separation such that it can fill its Roche lobe and form the disk. They provide a number of important constraints on the constituents of binaries which would lead to disk formation. The most likely system turns out to be an evolved AGB star with mass $2.5 < M_{agb}/M_{\odot} < 5$ for the primary, with a secondary of mass $\lesssim 0.08M_{\odot}$ and with an initial binary separation of $> 50 - 100R_{\odot}$ (Iben 1991). The AGB star will shed 80% of its mass during the common envelope ejection, leaving a post AGB stellar core of Mass M_c surrounded by a thin residual convective shell of mass M_e .

The time scale for the disk to move to its inner inner radius is of order or shorter than the viscous time scale. Even for systems with initial outer radii are of order $100R_{\odot}$, the relevant time scale would be no more than a few years. Since the disk would form only after the period of common envelope ejection, $< 1\text{yr}$, we would expect that the disk and the stellar shell to form concurrently within a time of order a few years. Because the relevant stellar field will be exposed once the envelope ejection occurs, and because any stellar dynamo growth time in the disk (discussed later) is less than 1 year, we expect the rotating stellar shell and disk to both be able to support co-operative jets at a time coincident within about a year after the disk forms. This represents the the initial time appearing in our calculations.

In section 2, we determine the MHD wind power from PPN stars and disks. This requires calcuation of the expected field strength in the disk and a model of how the accretion affects the stellar field. In section 3 we study the angular speed evolution of the stellar shell anchoring the stellar field, under the influence of accretion. In section 4 we derive expressions for the disk and stellar wnd luminosities. In section 5 we study cases for which the stellar shell is initially rapidly or slowly rotating, and calculate the effect on the maximum magnetic disk and stellar wind powers for each case. In section 6 we discuss the qualitative implications of the results in the context of PN. We briefly conclude in section 7.

2. Winds from Disks and Stars

There are many models of magnetic jet production and collimation in the literature. The extent and explicit details of collimation are less agreed upon than the principles of launching. The magnetic launch mechanism can be divided into two basic classes, “spring” mechanisms (Uchida & Shibata 1985; Contopoulos 1995 Lynden-Bell 1996) and “fling”

mechanisms (Blandford & Payne 1982; Lovelace et al. 1987). In the former class of models the initial driving force is a magnetic spring, i.e. the magnetic field energy density of order the kinetic energy density in the disk and the outflow is driven by toroidal field pressure. In the fling mechanisms, the initial driving is centrifugal along poloidal field lines. and later in the corona the wind becomes magnetically driven. In this study we focus simply on the total available magnetic luminosity L_m which we is greater or equal to to the wind luminosity. The L_m is the integral of the Poynting flux over the surface area of the rotator. This is

$$L_w \sim \dot{M}_w v_w^2 \lesssim L_m = \int (\mathbf{E} \times \mathbf{B}) \cdot d\mathbf{S} \sim \int_{R_i}^{R_o} (\Omega R) B_p B_\phi R dR, \quad (1)$$

where B_ϕ and B_p are the toroidal and poloidal field respectively, Ω and R are the rotational frequency and radius of the magnetized wind source, \dot{M} is the wind outflow rate, and v_w is the wind outflow speed. In what follows we discuss this equation in the context of PPN disks and post AGB stars. For all cases of interest for disks the integrand falls off fast enough such that it is the inner radius that matters. Thus for disks we have

$$L_{dw} \lesssim L_m \sim B_p(R_i) B_\phi(R_i) \Omega_d(R_i) R_i^3, \quad (2)$$

where Ω_d is the disk angular speed. For stars, we simply have

$$L_{sw} \lesssim L_m \sim B_p(R_*) B_\phi(R_*) \Omega_*(R_*) R_*^3, \quad (3)$$

where Ω_* is the angular speed of the stellar surface in which the field lines are anchored. The above magnetic wind luminosities are not independent. The poloidal and the toroidal fields are coupled through differential rotation in both the disk and star and the angular velocity of the star may depend on the accretion. In addition, the inner radius of the disk depends on the stellar magnetic field. Thus (2) and (3) are very much interdependent.

We now proceed to solve for the coupling relations and consider the stellar and disk MHD wind luminosities for two cases:

- The star is initially a strongly magnetized rotator independent of the accretion.
- The star is initially a slow rotator but is spun up by the disk accretion.

As we will see, the evolution in both cases depends on estimates of the disk and star magnetic fields. We must also solve for the disk inner radius, and the stellar surface angular speed evolution.

2.1. Magnetic Field of Disk

If the jet/wind is due to a magnetic field in the disk, this field must be produced in situ for the PN case. This is because the companion star, the progenitor of the disk, would have to be a brown dwarf or a Jupiter type planet (Reyes-Ruiz & Lopez 1999) which typically would only have fields of order or less than 10G. Even a field several orders of magnitude larger would be far too small to have any influence on the disk which forms from shredding this mass if the disk field were only that resulting from flux freezing. We estimate the field strength roughly from dynamo or turbulent amplification in the disk. An alternative dynamo approach to ours is given by Reyes-Ruiz & Stepinski (1995).

For an accretion disk whose angular momentum is transported by a magneto-shearing instability (c.f. Balbus-Hawley 1991, 1998), the time scale for growth of unstable modes, and the time scale for the largest eddy turnover time are both approximately equal to the rotation time scale. Very roughly, the eddy turnover time can be written as L/v_T where v_T is the dominant turbulent velocity and L is the dominant correlation scale. Since the field grows through shearing in the eddies we can estimate the strength of the mean magnetic field as follows. First we estimate the total magnetic energy. Using the Shakura-Sunyaev (1973) viscosity prescription

$$\nu = \alpha c_s H \sim v_T^2 / \Omega, \quad (4)$$

where α, c_s, H and Ω/v_T are the disk viscosity parameter, the sound speed, the scale height and the dominant eddy turnover time respectively. Using the fact that turbulent stretching leads to $v_A \sim v_T$, where v_A is the Alfvén speed, and $\Omega R = c_s R / H$ for a thin accretion disk, we then have straight away

$$v_A^2 = \alpha c_s^2. \quad (5)$$

When modeled as a mean-field dynamo $\alpha - \Omega$ dynamo (c.f. Parker 1979; Reyes-Ruiz & Stepinski 1995; Blackman 2000), it can be shown that due to the differential shear, the mean toroidal field exceeds the saturated mean poloidal field strength in the disk by a factor of H/L . From (4) and (5) we have $L \sim \alpha^{1/2} H$ and thus

$$B_p \sim \alpha^{1/2} B_\phi. \quad (6)$$

Whether this relation holds true in the base of the disk corona where the jet would launch is unclear but since the field in the corona is no greater than the field in the disk, the overall disk mean field provides a good upper limit at least to the total mean field energy density. Note that the total mean stress $\langle B_\phi B_p \rangle = \langle \bar{B}_\phi \bar{B}_p \rangle + \langle b_\phi b_p \rangle$, where the second term is a correlation of fluctuating fields. Actually, both of these terms can drive a wind. Exploring this point is outside the scope of the present paper, and here we simply stick with the

standard approach (e.g. Blandford & Payne 1982) where the large scale fields drive the wind. Thus we ignore the $\langle b_\phi b_p \rangle$ term.

The upper limit of the mean field is of order the random field, so from (5) we have, for the dominant disk field component

$$B_\phi^2 \sim 4\pi\rho_d\alpha c_s^2. \quad (7)$$

From the mass continuity equation for the disk we have,

$$\rho_d = \dot{M}_a / (4v_R\pi R^2), \quad (8)$$

where v_R is the radial infall speed. For (thin or ADAF) disks

$$v_R \sim \alpha c_s H/R \sim \alpha v_k (H/R)^2, \quad (9)$$

where $v_k^2 = GM/R$, the Keplerian speed. Then using (7) and (8) and (9), we have

$$B_\phi B_p = \alpha^{1/2} B_\phi^2 = \alpha^{1/2} v_k (R) \dot{M}_a / R^2. \quad (10)$$

This expression can be used to estimate either the magnetic field strength or Maxwell stress available in the disk for launching a wind.

2.2. Magnetic field of the stellar shell

The relevant stellar field is the surface field of the post AGB star. Observational interpretation suggests that the common envelope ejection, which would precede disk formation, removes $\sim 80\%$ of an initially $\sim 3M_\odot$ star (Schöberger 1993). Convective stellar models for a $3M_\odot$ star (Kawalar, private communication 2000) then tell us that outer layer will have a convective shell containing a mass of order $0.01M_\odot$. Thus we distinguish the core of the star M_c which will be the gravitational source of energy from the thin shell M_e . As we discuss below, it is the thin shell in which the stellar field will be anchored.

Since the convective shell is likely to be differentially rotating with respect to the core we assume that the shear rate is of order the shell's angular speed, Ω_* . The shear will stretch a dynamo produced poloidal field linearly in time. The linear stretching could operate coherently over a vertical diffusion time $\tau_D \sim R_*^2/\eta_T$, where $\eta_T \sim Lv_T$ is the turbulent diffusion coefficient for turbulent velocity v_T and scale L . (This may differ for interface dynamo models, c.f. Parker 1993; Markiel & Thomas 1999). Using numbers from Kawaler (private communication 2000), the diffusion time could be of order a few times the convective overturn time for the largest eddies in the post-AGB star, about 0.05yr. In any

case, for linear growth of the toroidal field, the toroidal and poloidal fields are then related by

$$B_{\phi*} \sim B_{p*} \Omega_* \tau_D, \quad (11)$$

which follows from the magnetic induction equation. Although the poloidal field B_{p*} will likely also depend on Ω_* , it will also depend on other properties of the turbulence and the mechanism of field origin (e.g. stellar dynamo, c.f. Parker 1979, 1993 for general reference; also see Pascoli 1997; Soker 1998). For an initial treatment of the problem, we simply consider B_{p*} as an input condition.

2.3. Disk inner radius

Now that we have the stellar magnetic field, we can calculate the disk inner radius. Related calculations were performed by Ghosh & Lamb (1978) and Ostriker & Shu (1995). We estimate the inner radius by balancing the infall ram pressure from the disk with the magnetic pressure of the star. For the infall velocity we use the free fall velocity, as that corresponds to the field strength at which the disc must absolutely truncate. Thus our calculation represents a lower limit on the inner radius. Note for example that when the Alfvén speed in the disk, using the stellar field strength, equals the sound speed there, magneto-shearing instabilities will be shut off. Thus at this field strength the nature of the angular momentum transport must change (to e.g. global modes, B.Chandran, E.Ostriker, 2000 personal communication). We assume that this change occurs and thus still use the larger Keplerian speed for the balance below.

Using the r^{-3} dependence for a dipole field and considering only the values at the equator $r = R$, we have

$$\frac{1}{4\pi} B_*^2 \left(\frac{R_*}{R_i} \right)^6 \simeq \rho_{d,i} v_{k,i}^2, \quad (12)$$

where $v_{k,i}$ is the Keplerian (\sim free-fall) speed at R_i . Note that when $\Omega_* \tau_D \gtrsim 1$, $B_*^2 \sim B_{\phi*}^2$, otherwise $B_*^2 \sim B_{p*}^2$. This is important because the angular speed couples in the former case but not in the latter.

The next step is to use the mass continuity equation (8) for R_i . The result is

$$R_i = B_*^{4/7} (1 + \Omega_{T*} \tau_D)^{4/7} R_*^{12/7} (GM_c)^{-1/7} \dot{M}_a^{-2/7} = B_{p*}^{4/7} R_*^{12/7} (GM_e)^{-1/7} \dot{M}_a^{-2/7}, \quad (13)$$

The inner radius will be time dependent because of the time dependent accretion rate and the angular speed of the stellar shell. We compute the evolution of the angular speed next.

3. Angular Speed of the Star

The disk and stellar wind luminosities depend on the angular velocity Ω_* of the stellar convective shell where the field is anchored. As shown above Ω_* is one factor which determines the magnetic pressure of the star, and thus the inner radius of the disk. Only for extremely large τ_D is the magnetic pressure determined by B_{p*} . In that case Ω_* decouples from R_i .

If material is accreting onto the star from the disk at expected rates based on the disk formation models of Reyes-Ruiz and Lopez (1999), then

$$\dot{M}_a \sim 6 \times 10^{22} \left(\frac{t}{1\text{yr}} \right)^{-5/4} \text{g/sec}, \quad (14)$$

and there may be some contribution to the rotation of the convective shell from the accreted material. There are many complications features of this accretion process. Here we simply assume that the material imparts its angular momentum to the shell (e.g. via the magnetic field) as it accretes. We also assume that the accreted material does not change the thickness of the outer convective layer. The rotation speed of the relevant stellar envelope is then determined by balancing the angular momentum gained from the accretion with that lost from the MHD wind. We have the following approximate equation

$$M_e \frac{d\Omega_* R_*^2}{dt} = -\dot{M}_a \Omega_* R_*^2 + \dot{M}_a \Omega_{k,i} R_i^2 - B_{p*}^2 \Omega_* R_*^3 \tau_D. \quad (15)$$

where M_e is the shell mass, Ω_* is the shell angular speed, $\Omega_{k,i}$ is the Keplerian angular speed at the disk inner edge, and we have assumed a constant R_* . The last term on the right hand side is due to the magnetic torque applied by the wind ($\propto B_{p*} B_{\phi*}$). This equation applies when R_i corresponds to a radius at which the disk is spinning faster than field lines of the star (assumed to be rigidly attached to the star) at that radius. Thus it is assumed that the disk accretion can spin up the stellar convective envelope. There exists a regime in which the star spins fast enough to disrupt the disk, and angular momentum of the star is lost to the disk. We do not consider that regime. Note further that if R_i were greater than the radius at which the corotation speed exceeded the Keplerian speed of the star, there would be no accretion (Armitage & Clarke 1996).

Re-arranging, and expanding the Keplerian term, we have

$$\frac{d\Omega_*}{dt} + \Omega_* (\dot{M}_a/M_e + B_{p*}^2 R_* \tau_D/M_e) \simeq \frac{(GM_c)^{1/2} \dot{M}_a R_i^{1/2}}{R_*^2 M_e}. \quad (16)$$

In the simple limit of no disk, only the 1st and 3rd terms of (16) would contribute and the solution would be

$$\Omega_* = \Omega_{*0} e^{-t/t_m}, \quad (17)$$

where we define the magnetic spin-down timescale t_m

$$t_m = \frac{M_e}{B_{p*}^2 R_* \tau_D}. \quad (18)$$

This quantity is the spin down time from MHD powered rotational energy loss. For typical parameters, t_m scales as

$$t_m \sim 50 \left(\frac{M_e}{10^{-2} M_\odot} \right) \left(\frac{B_{p*}}{1 \text{kG}} \right)^{-2} \left(\frac{R_*}{10^{-11} \text{cm}} \right)^{-1} \left(\frac{\tau_D}{10^5 \text{sec}} \right)^{-1} \text{yr} \quad (19)$$

As we shall see there are two regimes of interest to pursue in analytic approximation depending on whether t/t_m is large or small.

For the kind of disks considered here, the second term in (16) can be ignored compared with the third. Also, for the maximum accretion rates we consider (*i.e.* $\sim 10^{-3} M_\odot \text{yr} (t/1\text{yr})^{-5/4}$), a mass shell of $0.01 M_\odot$ will at most have a 30% gain in mass over the lifetime, because of the form of the time dependence, so we can assume M_e is a constant. The ODE can then be solved by standard integrating factor techniques (and is in fact analogous to an RL circuit). We find

$$\Omega_* = C \text{Exp} \left[- \int^t \frac{dt'}{t_m} \right] + \text{Exp} \left[- \int^t \frac{dt'}{t_m} \right] \times \int^t \text{Exp} \left[\int^t \frac{dt}{t_m} \right] q(t') dt' \quad (20)$$

where we define

$$q(t) = \frac{(GM_c)^{1/2} \dot{M}_a(t) R_i^{1/2}(t)}{R_*^2 M_e}. \quad (21)$$

We do not consider the solution before $t = 1\text{yr}$ when the accretion disk is still forming. For the approximate early time solution, $t/1\text{yr} < t/t_m << 1$, we set the exponentials equal to 1. The result (after the 1 yr disk formation grace period) is then

$$\Omega_*(t) \simeq \Omega_{*0} + \omega_0 \left(1 - \left(\frac{t}{1\text{yr}} \right)^{-1/14} \right), \quad (22)$$

where

$$\omega_0 = \frac{3 \times 10^8 (GM_c)^{1/2} \dot{M}_{a0} R_{i0}^{1/2}}{R_*^2 M_e} \quad (23)$$

where we have taken Ω_{*0} , as the initial angular speed of the residual stellar convective shell in which the field is anchored. We have ignored the time dependence in R_i from Ω_* , while including the implicit time dependence from \dot{M}_a . This is a good approximation for this

regime because $R_i^{1/2}$ depends on $\Omega_*^{2/7} \dot{M}_a^{-1/7}$. Note that expression (22) allows us to define the difference between initially fast ($\Omega_{*0} > \omega_0$) and slow ($\Omega_{*0} < \omega_0$) stellar rotation.

When $t/t_m > 1$ the exponential in (20) begins to evolve quickly compared to the power law decay of the $\dot{M}_a R_i^{1/2}$ factor inside the last integral. Factoring this out and noting that the product of integrals in this last term then cancel we then have

$$\Omega_*(t) \sim q(t)t_m + (K - q(t)t_m) e^{(-t/t_m)}, \quad (24)$$

where $K = e\Omega_*(t_m) + q(t_m)t_m(1 - e)$. For large times ($t/t_m > 1$) the first term on the right of (24) dominates and we have

$$\Omega_*(t) \simeq q(t)t_m = \frac{(GM_c)^{1/2} \dot{M}_a R_i^{1/2}}{B_{p*}^2 R_*^3 \tau_D} = \frac{(GM_c)^{3/5} \dot{M}_a^{6/5}}{B_{p*}^{12/5} R_*^3 \tau_D}, \quad (25)$$

where the latter equality follows from the fact that R_i depends on Ω_* from (13). Note that (25) should be used only when it produces a value below the corresponding escape speed.

4. Disk Wind Luminosities

Plugging (10) into (2), we have

$$L_{dw} = \dot{M}_w v_{dw}^2 = \alpha^{1/2} \int B_\phi^2 \Omega_{k,i}^2 R dR \sim \alpha^{1/2} \dot{M}_a G M_c / R_i. \quad (26)$$

We now consider several cases which involve using the appropriate value of R_i from section 2.3 in (26), then using the appropriate solution for Ω_* from section 3 in the equation for R_i . We will also use (14) for \dot{M}_a .

We first consider the case where stellar rotation is low ($\Omega_{*0} < \omega_0$). The maximally luminous case will have the smallest disk inner radius. For a given poloidal field, the toroidal stellar field will be weakest for slowly rotating stars as per our discussion above. Thus in this case the disk inner radius will be the smallest. When R_i as calculated from section 2.3 satisfies $R_i \leq R_*$, we use $R_i = R_*$ and the disk luminosity is given by

$$L_{dw} \simeq \frac{\alpha^{1/2} G M_c \dot{M}_a}{R_*} \sim 10^{36} \frac{\alpha_{-2}^{1/2} \dot{M}_{a0,22} M_{c,1}}{R_{*,11}} \left(\frac{t}{1\text{yr}} \right)^{-5/4} \text{erg/sec.} \quad (27)$$

In this and the expressions which follow we scale α to 0.01, magnetic fields to 10^3 G, radii to 10^{11} cm, diffusion times to 10^5 yr, stellar core masses to $1 M_\odot$, stellar shell masses to $10^{-2} M_\odot$, angular speeds to 10^{-4} Hz and mass loss rates to 10^{-22}gs^{-1} . These scalings are indicated by the subscripts.

We now consider the case of an initially rapidly spinning star. The disk and star are strongly coupled through R_i and we must consider the different temporal regimes relative to the ratios t/t_m and $\Omega_*\tau_D$. When $t < t_m$ the first term on the right hand side of (22) dominates and using (13) we have

$$L_{dw} \simeq \frac{\alpha^{1/2}(GM_c)^{8/7}\dot{M}_a^{9/7}}{B_{p*}^{4/7}\tau_D^{4/7}\Omega_*^{4/7}R_*^{12/7}} \sim 10^{36} \frac{\alpha_{-2}^{1/2}M_{c,1}^{8/7}\dot{M}_{a0,22}^{9/7}}{(B_{p*,3}\tau_{D,5}\Omega_{*0,-4})^{4/7}R_{*,11}^{12/7}} \left(\frac{t}{1\text{yr}}\right)^{-45/28} \text{erg/s.} \quad (28)$$

For $t > t_m$, using (13) (under the assumption that $B_{\phi*} \gtrsim B_{p*}$), and (25) in combination with (26), we have

$$L_{dw} \simeq \alpha^{1/2}(GM_c)^{4/5}\dot{M}_a^{3/5}B_{p*}^{4/5} \sim 10^{34}\alpha_{-2}^{1/2}M_{c,1}^{4/5}\dot{M}_{a0,22}^{3/5}B_{p*,3}^{4/5} \left(\frac{t}{50\text{yr}}\right)^{-3/4} \text{erg/s} \quad (29)$$

In the limit that $\Omega_*\tau_D < 1$, which would occur for late times, $B_{p*} > B_{\phi*}$, and from (13) we obtain,

$$L_{dw} \sim \frac{\alpha^{1/2}(GM_c)^{8/7}\dot{M}_a^{9/7}}{B_{p*}^{4/7}\tau_D^{4/7}\Omega_*^{4/7}R_*^{12/7}} \sim 10^{32} \frac{\alpha_{-2}^{1/2}M_{c,1}^{8/7}\dot{M}_{a0,22}^{9/7}}{B_{p*,3}^{4/7}R_{*,11}^{12/7}} \left(\frac{t}{500\text{yr}}\right)^{-45/28} \text{erg/s.} \quad (30)$$

4.1. Stellar wind luminosities

The stellar wind luminosity is given by (3). We note again the hidden dependence of the field on the rotational velocity. If a dynamo generates the stellar field, then both B_p and B_ϕ can depend on Ω_* . For example the rotation would be required to generate the pseudoscalar helicity that sustains a steady field in dynamo models. Also, the toroidal field may induce poloidal field by springing outward. More subtle dependences should be considered in future work, but the important point here is the recognition of some dependence on the rotation, and thus on the supply of angular momentum from the disk. Here we simply assume that the poloidal field of the star is kept at a constant value either by a dynamo or by buoyancy of toroidal field, while the toroidal field also depends linearly on the rotational speed as implied by growth from shear. In this case, equation (3) gives

$$L_{sw} \sim B_{*p}B_{*\phi}\Omega_*R_*^3 \sim B_{p*}^2\Omega_*^2\tau_D R_*^3. \quad (31)$$

We now consider the same temporal regimes for the stellar wind power that were examined for the disk wind. For a rapidly rotating star in the $t < t_m$ regime, the first term on the right hand side of (22) is dominant and from (31) we then have,

$$L_{sw} \simeq B_{p*}^2\Omega_{*0}^2\tau_D R_*^3 = 10^{36}B_{p*,3}^2\Omega_{*0,-4}^2\tau_{D,5}R_{*,11}^3 \text{ erg/s.} \quad (32)$$

For a very slowly rotating star in the $t < t_m$ regime, the second term on the right of (22) is dominant. The spin evolves to with in a factor of 1/10 of ω_o after a few years. In this case Ω_* is such that R_i from (13) is less than R_* so we take $R_i = R_*$. The stellar rotation rate and wind power thus approach

$$\Omega_* \sim (3 \times 10^7) \sqrt{\frac{GM_c \dot{M}_{a0}^2}{R_*^3 M_e^2}} \quad (33)$$

and

$$L_{sw} \sim 3 \times 10^{33} \frac{B_{p*,3}^2 \tau_{D,5} M_{c,1} \dot{M}_{a0,22}^2}{M_{e,-2}} \text{ erg/s.} \quad (34)$$

respectively. The slow time evolution in (22), which results in the approximation that the angular speed and luminosity are constant in (33) and (34), reflects the fact that during this period the angular momentum gain from accreted material and the loss of angular momentum from the wind nearly balance.

For $t > t_m$, but for $\Omega_* \tau_D > 1$, using (25) and (13) with (31), we have

$$L_{sw} \sim \frac{(GM_e)^{6/5} \dot{M}_a^{12/5}}{B_{p*}^{14/5} R_*^3 \tau_D} = 4.7 \times 10^{33} \frac{M_{c,1}^{6/5} \dot{M}_{a0,22}^{12/5}}{B_{p*,3}^{14/5} R_{*,11}^3 \tau_{D,5}} \left(\frac{t}{50 \text{yr}} \right)^{-3} \text{ erg/s} \quad (35)$$

For late times when $\Omega_* \tau_D < 1$, we have

$$L_{sw} \sim \frac{(GM_e)^{6/7} \dot{M}_a^{12/7}}{B_{p*}^{10/7} R_*^{9/7} \tau_D} = 10^{31} \frac{M_{c,1}^{6/7} \dot{M}_{a0,22}^{12/7}}{B_{p*,3}^{10/7} R_{*,11}^{9/7} \tau_{D,5}} \left(\frac{t}{500 \text{yr}} \right)^{-15/7} \text{ erg/s.} \quad (36)$$

5. Slow and Rapid Initial Stellar Rotation Cases

We now separately consider the cases for which the initial spin of the stellar shell is negligible, and the case for which the stellar shell is spinning rapidly.

Slow Rotation: In fig 1a and 1b we present plots of L_{dw}/L_{sw} for the slow rotator case ($\Omega_{*0} < \omega_0$). Those figures show the first two of the three time regimes we now discuss.

The first regime is for $t < t_m$. We can see from (27) and (34) that the disk wind luminosity initially dominates the stellar wind luminosity by several orders of magnitude. The disk wind then falls off as $t^{-5/4}$. The stellar wind luminosity on the other hand experiences a slow growth up to $t \sim t_m$. This can be seen in our approximate relations for L_{dw} and L_{sw} in this regime which show the stellar wind coefficient 4.7×10^{33} at $t > t_m$ in (35) is greater than the coefficient of 3×10^{33} when $t < t_m$.

After $t > t_m$, Eqn. (35) shows that the stellar wind falls off rapidly (t^{-3}). From (29) we see that the disk wind luminosity only falls off as $t^{-3/4}$. This change in time dependence of the disk wind luminosity occurs because, after $t > t_m$, the stellar wind angular velocity is dropping rapidly, slowing the outward evolution of R_i (equation 13). The toroidal stellar field is no longer increasing significantly.

The third regime, not shown in the figures since the winds are likely to be quiescent by this time, begins when $\Omega_*\tau_D < 1$. Here the poloidal field of the star dominates the pressure. The angular velocity and the inner disk radius become decoupled so the decreasing accretion rate is less influential on the angular momentum of the star while the disk wind inner radius is moving outward more quickly with time than at earlier times. In this asymptotic regime the stellar wind power falls as $t^{-2.1}$ and the disk wind luminosity falls as $t^{-1.6}$.

Thus, for small Ω_{*0} , the disk wind first dominates the stellar wind. The stellar wind grows in power slightly whereas the disk wind power falls. As a result, the stellar wind power approaches and nearly equals the disk wind power near $t \sim t_m$. Afterward, the stellar wind falls rapidly and the disk wind always falls more slowly than the stellar wind. The disk wind also dominates at large times. *The star is therefore slaved to the disk throughout the evolution in this slow rotator case.* The wind and spin axes of the star are also slaved to those of the disk because the toroidal field is stretched perpendicularly to the axis of rotation and the wind emanates perpendicularly to the toroidal field. The disk and stellar winds would thus be coaxial.

Rapid Stellar Rotation: In fig 1c and 1d we present plots of L_{dw}/L_{sw} for the rapid rotator case ($\Omega_{*0} > \omega_0$). Again the first two of the three time regimes are shown. For $t < t_m$, the disk wind luminosity $\lesssim 10^{36}(t/1\text{yr})^{1.6}$ erg/s from (28) and the stellar wind is essentially a constant $\lesssim 10^{36}$ as seen in (32). Note that here the maximum stellar wind and disk luminosities can be initially comparable. If the star is spinning nearly at break up speed, the stellar wind luminosity can dominate that of the disk until $t \sim t_m$. After this time the the angular speed of the star drops rapidly and the disk wind dominates. The evolution for $t > t_m$ is the same as for the small Ω_{*0} case.

Thus for the large Ω_{*0} case, the stellar wind is independent of the disk until $t = t_m$. After this time its MHD wind luminosity is negligible compared to that of the disk. (If there were no disk at all, one would see only the rapid fall of of the stellar wind as in equation (17)). The initial independence of the star from the disk means that the axes of the two winds can be misaligned. The origin of the stellar spin and magnetic axes are decoupled since the spin axis of the disk is independently determined by the initial plane of the binary orbit. Thus the disk and stellar wind system can produce a multipolar wind system of up to $\sim 10^{36}$ erg/s.

6. Discussion

Our results show that powerful magneto-centrifugal winds can be driven in PNe systems. In addition, in the context of accretion disks formed from the break-up of a secondary star in a binary system, these winds are time dependent and have a finite lifetime. Thus our model would predict that transient, strongly collimated flows can be driven during the transition from AGB to PNe. This is very much in line with what has been inferred from observations of PPNe (Sahai & Trauger 1998). The use of winds driven by magneto-centrifugal forces solves two problems which have emerged from PNe studies (Frank 2000). First, they explain how strong flows can be driven before the star becomes hot enough to produce a radiative line-driven wind. Second, they provide the ingredients to explain the high degree of collimation seen in some sources. Our hybrid star+disk wind scenario, may account for multiple shells or multipolar outflows within the MHD framework. Below we summarize our main points and discuss the morphologies which might result:

Summary: We have derived maximal disk and stellar MHD wind powers for a coupled disk-star system at times $t < t_m$, $t > t_m$ and for values of $\Omega_* \tau_D < \text{or} > 1$ and $\Omega/\omega_0 < \text{or} > 1$. Our calculations take the initial time to be the onset of disk formation in a binary system from common envelope expulsion. For PNe, the initial onset of the star and disk wind should be nearly contemporaneous. The layers of the star with the strong magnetic field that power the wind are only exposed after the common envelope is ejected, while the accretion disk forms within a year from the common envelope ejection.

The resulting luminosities for both winds depend only on the disk accretion rate and properties of the star. This is because the inner regions of the disk are the main contributor to the disk wind and the inner disk radius is determined by the properties of the star. We determined the magnetic field strength in the disk by analytic relations derived from consequences of magneto-shearing instability driven disk turbulence. The magnetic field strength in the star was assumed to be a combination of a steady stellar poloidal field, and a strengthening of the toroidal component due to angular velocity shear in the stellar envelope. Two distinct evolutionary schemes arise depending on the initial spin of the envelope. The late time wind luminosities are, however, independent of this initial spin rate.

We now summarize some numbers and consequences for the maximum wind powers.

* For our choice of fiducial scalings, the luminosity of a stellar wind from an initially rapidly rotating post AGB star with typical field strengths $\sim 10^3$ Gauss, initially satisfies $L_{sw} \lesssim 10^{36}$ erg/sec, and is approximately constant in time. During this time, the disk wind

satisfies $L_{dw} \lesssim 10^{36}(t/1\text{yr})^{-1.6}$ as the accretion rate falls.

- * After t_m , $L_{sw} \lesssim 5 \times 10^{33}(t/50\text{yr})^{-3}$, and the disk wind power flattens to $L_{dw} \lesssim 10^{34}(t/50\text{yr})^{-3/4}$. The flattening occurs because the rapid fall in the shell spin means that the toroidal field is no longer rapidly amplifying. This slows any increase in the magnetic pressure from the toroidal field and the inner radius of the disk slows its evolution outward. It could actually move inward. This somewhat compensates for the decreasing accretion rate since the disk power is always dominated by the contribution from the inner disk radius.
- * When $t > 10t_m$, $L_{dw} \lesssim 10^{33}(t/500\text{yr})^{-1.6}\text{erg/s}$, and the angular speed is so low that the inner radius is determined only by the decreasing accretion rate and the stellar poloidal field without the extra dependence on the stellar rotation. The time dependence steepens as the radius moves outward more rapidly. In this regime, $L_{sw} \lesssim 10^{31}(t/500\text{yr})^{-15/7}\text{erg/s}$. Here the stellar wind power slightly flattens but is still steeper than that of the disk wind.
- * Whilst the dominance of disk vs. stellar wind depends on Ω_{*0} for $t < t_m$, for all $t > t_m$, the disk wind always dominates, regardless of Ω_{*0} ,

Observational Consequences: The shape of an outflow driven by our hybrid model will depend on the initial rotation rate as discussed. There are two other parameters which likely play a role. The ratio of the spin-down time t_m and the transition time for the star to become a PN nucleus t_{PN} will determine how much of shaping will be controlled by the combined star+disk wind. When $t_m/t_{PN} \ll 1$, the results of the hybrid winds are likely to appear as microstructures such as knots, bullets, or ansae in a mature PNe. When $t_m/t_{PN} \gtrsim 1$ then structures such as multipolar bubbles which develop during the period when $L_{dw} \approx L_{sw}$ may leave a large enough imprint to survive into the PN phase.

The other important parameter is the ratio of the thrust, $\Pi = \dot{M}V$, along the central wind axis for each of the two winds. This will be proportional to the ratio of the terminal wind speeds (V_{dw}/V_{sw}) and will depend on collimation. While the terminal velocity of the winds will always be of order the observed wind speed, the actual magnitude will depend on the details of the wind launching process. Thus it is not unreasonable to imagine the winds to differ by a factor of a few one way or the other. The ratio $\Pi_{dw}/\Pi_{sw} \propto V_{dw}/V_{sw}$ will determine the shape of the resulting outflow by determining which wind-driven “lobe” extends farther.

When $\Pi_{dw}/\Pi_{sw} > 1$ and the star is slowly rotating ($\Omega_{*0} < \omega_o$) then we expect two nested aligned bipolar bubbles. Such a shape is shown in Fig 2a. An example of a PNe with this shape is Hubble 12 (Welch *et al.* 1999). In the case where the star is initially rapidly rotating and the stellar and disk magnetic and rotational axes are not aligned then a nested

multi-polar bubble may emerge as is shown in Fig 2c. An example of such an outflow is M2-46 (Manchado 2000).

When $\Pi_{dw}/\Pi_{sw} < 1$ and the star is rapidly rotating ($\Omega_{*o} < \omega_o$) then the stellar wind will push ahead of the disk wind and may produce the jet-like features seen in NGC 7007 (Fig 2b, Balick *et al.* 1998). In the case where the star is initially rapidly rotating and the stellar and disk axes are not aligned then a second form of nested multi-polar bubble may emerge as is shown in Fig 2d. An example of such an outflow is He2-155 (Sahai 2000).

Note also that in the rapidly rotating case, due to differences in time dependence, one would observe one set of bipolar lobes (those from the star) to be continuous from the source, while the other (from the disk) would appear as antipodal knots. This would occur in the rapid stellar rotation case because the disk wind power falls while the stellar wind does not during the $t < t_m$ regime. Such a signature of the combination of disk and stellar wind may be manifest in the Egg nebula (Jura *et al.* 2000).

Given that typical sound speeds for observed outflows are of order 20-30 km/s, while the wind velocities can be > 100 km/s one can estimate the size of outflow structures compared with the distance from the star. For a hybrid outflow with strongest power phase lasting only \sim few years, but with an age or order hundreds of years, one should see knots (or shells depending on collimation) which with a width of order 10^{16} cm. If the outflow velocity were 100 km/s, then the knot/shell distance from the central core would be ~ 5 times the shell thickness. Such features are seen in the Cat's Eye nebula (Miranda & Solf 1992)

Finally we note that either the disk or the star could precess thus leading to an additional point symmetry (see also Manchado *et al.* 1996). In addition, the interaction of the stellar and disc winds may lead to extra symmetries due to edge features or formation of shocks. Further study is needed. We also note that except for the functional form of the accretion rate, \dot{M}_a our qualitative picture calculation could be applied to other coupled disk+star systems. This would include outflows in PN systems in cases where a secondary accretes matter from the primary (Soker & Livio 1994, Mastrodemos & Morris 1998). Finally we note that in all cases a dynamo in either a disk or the star or both may be responsible for the field driving the wind. Magnetic flaring and the production of hard X-rays can then be expected in PPN systems. Observations of PPN systems with Chandra and other X-ray telescopes would therefore be highly desirable.

7. Conclusions

Our study highlights the importance of understanding the interplay between MHD disk winds vs. MHD stellar winds in explaining the diversity of observed outflows in planetary nebulae.

We find that MHD disk winds dominate the stellar winds for $t > t_m$ regardless of the initial stellar spin rate, and the star is slaved to the disk. For $t < t_m$, the stellar wind power can be comparable to that of the disk, even exceeding it if the star is initially rotating fast enough. The stellar wind can emanate along a different symmetry axis than the disk wind in this regime and bipolar outflows can be produced. For a rapidly rotating star, the stellar MHD wind power is steady for a time of order $t = t_m$, meanwhile the disk wind power falls rapidly. For $t > t_m$, the disk wind power falls off weakly, while the stellar wind power drops rapidly.

Generally, we would suggest that if a sustained MHD driven bipolar outflow extending to the core lasts for > 1000 yr, a disk is likely involved. (Note that the choice of scalings we use in the text were mainly to provide a general framework. The spin down time t_m could be longer than our scale of 50 years depending on radius and stellar convective diffusion time, (c.f. eqn (18)). Disk winds would further imply initial formation from a binary system. An initially rapidly rotating star would slow down rapidly by this time, and would only be able to contribute significantly if its wind were radiatively driven. If a stellar wind operates powerfully during $t < t_m$ it means that the central star was initially rotating rapidly.

There is no guarantee that a binary system would form, or that the star would be initially rapidly rotating for every post AGB star. Thus for all systems with bipolar outflows, observations that can reveal the rotation rate of the central star, its magnetic field, or the presence of binary companions are ultimately essential for testing MHD disk/stellar wind paradigms. Further studies of the disk wind-stellar wind interplay are most certainly needed. Given the ubiquity of the accretion-central object-outflow connection throughout the universe the same kind of investigation may ultimately be important for other stellar and compact object accretion systems as well.

Acknowledgements: E.B. was supported in part by NSF grant PHY94-07194 at the ITP, and thanks R. Krasnolpolsky, R. Blandford, B. Chandran, and E. Ostriker for discussions.

Figure Captions

Figure 1: Plot of the MHD wind power ratio for the disk and star for four regimes: a) $t < t_m$ for the initially slowly rotating star b) $t > t_m$ for the initially slowly spinning star c) $t < t_m$ regime for initially fast rotating star. d) $t > t_m$ regime for initially fast rotating star. The two late time evolutions (b and d) are expected to be the same as shown.

Figure 2: Qualitative comparison between HST PN images and schematic multipolar wind structures from the hybrid stellar-disc wind paradigm, for different initial stellar spins and thrust ratios Π_{dw}/Π_{sw} (see text). a) top left: $\Omega_{*0} < \omega_0$ and $\Pi_{dw}/\Pi_{sw} > 1$ so star is slaved to disk and the only possibility is nested winds. Inset is PN Hubble 12 (Welch *et al.* 1999). b) top right: $\Omega_{*0} < \omega_0$ and $\Pi_{dw}/\Pi_{sw} < 1$. Inset is NGC 7007 (Balick *et al.* 1998). c) bottom left: $\Omega_{*0} > \omega_0$ and $\Pi_{dw}/\Pi_{sw} > 1$. Inset is M2-46 (Manchado *et al.* 2000). d) bottom right: $\Omega_{*0} > \omega_0$ and $\Pi_{dw}/\Pi_{sw} < 1$. Inset is He2-155 (Sahai 2000).

References

Armitage P.J. & Clarke C.J., 1996, MNRAS, 280, 458.

Balick, B. 1987, AJ, 94, 671

Balick B., in *Asymmetrical Planetary Nebulae II*, 2000 J.H. Kastner, N. Soker, & S. Rappaport eds., ASP Conf. Ser. Vol. 199., pg 41

Balick, B; Alexander, J., Hajian, A., Terzian, Y, Perinotto, M., Patriarchi, P., 1998, AJ, 116, 360

Balbus S.A. & Hawley J.F., 1991, ApJ , 376 214.

Balbus S.A. & Hawley J.F., 1998, Rev Mod Physics, 72 1.

Blackman E.G., Yi I., Field G.B., 1996, ApJ, 473, L79.

Blackman E.G., Yi I., Field G.B. 1996, ApJ,

Blandford R.D. & Payne D.G. 1982, MNRAS, 199 883.

Blandford R.D., 2000, in “Proc of Discusison Meeting on Magnetic Activity in Stars, Discs and Quasars.”, Ed. D. Lynden-Bell, E. R. Priest and N. O. Weiss. To appear in Phil. Trans. Roy. Soc. A

Chevalier, R., & Luo, D., 1994, ApJ, 421, 225

Contopoulos J., 1995, ApJ 450 616.

Ferrari A., 1998, ARAA, 36 539.

Frank A., New Ast. Rev., 43, p31.

Frank, A., in *Asymmetrical Planetary Nebulae II*, 2000 J.H. Kastner, N. Soker, & S. Rappaport eds., ASP Conf. Ser. Vol. 199., pg 225

Frank J., King A., Raine D., 1992, “Accretion Power in Astrophysics” (Cambridge: Cambridge Univ. Press).

Garcia-Segura, G., 1997, ApJ, 489L, 189

Garcia-Segura G., Langer N., Rozyczka, M. & Franco J., 1999, ApJ 517 767.

Ghosh P.& Lamb F.K., 1978, ApJ 223, L83.

Iben I., 1991, ApJS 76, 55.

Iben I. & Livio M., 1993, PASP 105, 1373.

Icke, V., 1988, A&A, 202, 177

Jura M., Turner J. L., Van Dyk S., & Knapp G.R., 2000, ApJ, 528 L105.

Kahn, F. D., & West, K. A., 1985, MNRAS, 212, 837

Königl, A., & Ruden, S.P. 1993, in "Protostars and Planets III", ed. E.H. Levy & J.I. Lunine (University of Arizona Press), 641.

Kwok, S., Purton, C., Fitzgerald, P. M., 1978, ApJ 219, L125

Lovelace R.V.E., Wang J.C.L., Sulkhanen M.E., 1987 ApJ, 315 504.

Lovelace R.V.E., Romanova J.C.L., Bitsnovatyi-Kogan G.S., 1987 ApJ, 315 504.

Lynden-Bell D., 1996, MNRAS, 279 389.

Manchado A., Stanghellini L, Guerrero M.A., 1996, ApJ, 466 L95.

Manchado A., Villaver, E., Stranghellini, L., Guerrero, M., in *Asymmetrical Planetary Nebulae II*, 2000 J.H. Kastner, N.Soker, & S. Rappaport eds., ASP Conf. Ser. Vol. 199, pg 17

Mastrodemos, N., Morris, M., 1998, ApJ, 497, 303

Markiel J.A. & Thomas J.H., 1999, ApJ, 523 827.

Mészáros, P., & Rees, M.J. 1997, Ap.J. 482, L29

Miranda L.F. & Solf J., 1992, A&A 260 397.

Mirabel I.F. & Rodriguez L.F., 1999, ARAA, 37 409.

Morris, M. 1987, PASP, 99, 1115

Ostriker E.C. & Shu F.H., 1995, ApJ, 447, 813

Osterbrock, D., 1989, *Astrophysics of Gaseous Nebulae and Active Galactic Nuclei*, (University Science Books, CA)

Parker E.N., *Cosmical Magnetic Fields* (Oxford Univ Press: Oxford) 1979.

Parker E.N., 1993, ApJ, 408, 707.

Pascoli G., 1997, ApJ, 489, 946.

Pudritz, R.E. 1991, in "The Physics of Star Formation and Early Stellar Evolution", eds. C.J. Lada and N.D. Kylafis, NATO ASI Series (Kluwer), pg 365.

Pellitier G. & Pudritz R.E., 1992, ApJ, 394 117.

Reyes-Ruiz M. & Lopez J.A., 1999, ApJ, 524 952.

Reyes-Ruiz M. & Stepinksi T.F., 1995, ApJ, 438 750.

Rozyczka, M., & Franco, J., 1996, ApJ, 469, 127

Sahai, R., & Trauger, J. T. 1998, AJ, 116, 1357

Sahai, Raghvendra; Trauger, John T., Watson, Alan M., Stapelfeldt, Karl R., Hester, J. J., Burrows, C. J., Ballister, G. E., Clarke, J. T., Crisp, D., Evans, R. W., Gallagher, J. S., III; Griffiths, R. E., Hoessel, J. G., Holtzman, J. A., Mould, J. R., Scowen, P. A., Westphal, J. A., 1998, ApJ, 493, 301

Sahai, R., in *Asymmetrical Planetary Nebulae II*, 2000 J.H. Kastner, N. Soker, & S. Rappaport eds., ASP Conf. Ser. Vol. 199, pg 209.

Schönberner D., 1993, in IAU Symp 155, *Planetary Nebulae* ed. R. Weinberger & A. Acker (Dordrecht: Kluwer) 415.

Shakura N.I. & Sunyaev R.A., 1973, A&A 24 337.

Shu F.H., Najita J., Ostriker E., Wilkin F., Ruden S., Lizano S., 1994, ApJ 429 781.

Smith M.D., 1998, Ap&SS 261 169.

Soker, N., Livio, M., 1994, ApJ, 421, 219

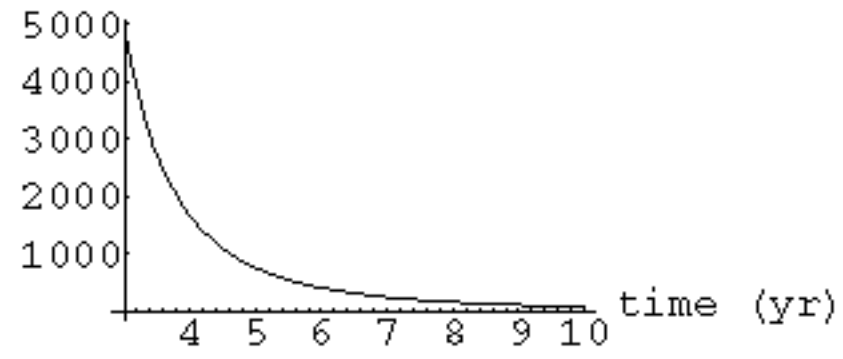
Soker N., 1998, MNRAS, 299, 1242.

Uchida Y. & Shibata K. 1985, PASJ, 37 31.

Usov V.V., 1992, Nature, 357, 472

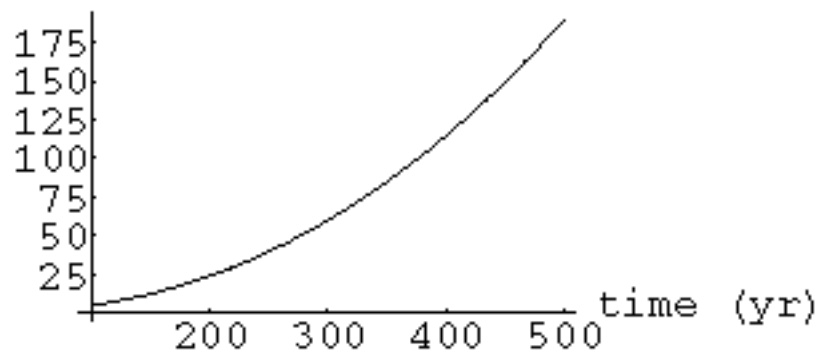
Welch, C., Frank, A., Pipher, J., Forrest, W., Woodward, C., 1999, ApJ, 522L, 69

$L_{\text{dw}}/L_{\text{sw}}$ (small Ω_{s0})



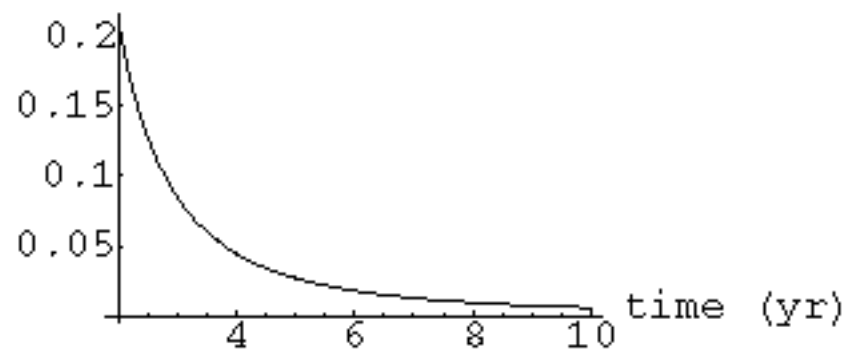
(a)

$L_{\text{dw}}/L_{\text{sw}}$ (small Ω_{s0})



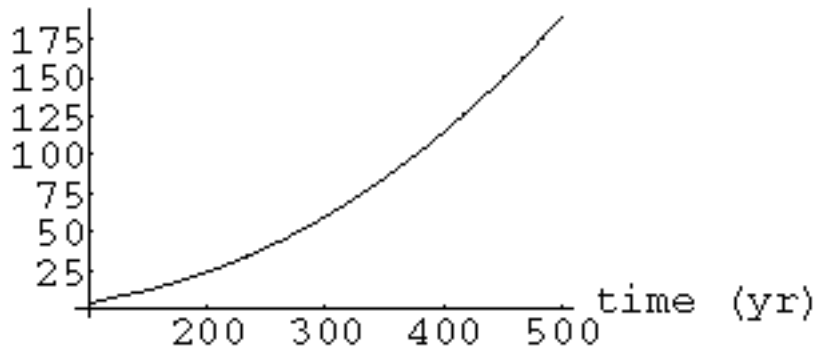
(b)

$L_{\text{dw}}/L_{\text{sw}}$ (large Ω_{s0})



(c)

$L_{\text{dw}}/L_{\text{sw}}$ (large Ω_{s0})



(d)

This figure "Fig2all.jpg" is available in "jpg" format from:

<http://arxiv.org/ps/astro-ph/0005288v2>